

Cite this: *Nanoscale Adv.*, 2019, 1, 961Received 22nd October 2018  
Accepted 19th November 2018

DOI: 10.1039/c8na00300a

rsc.li/nanoscale-advances

# Enabling the electrocatalytic fixation of N<sub>2</sub> to NH<sub>3</sub> by C-doped TiO<sub>2</sub> nanoparticles under ambient conditions†

Kun Jia,<sup>ab</sup> Yuan Wang,<sup>ab</sup> Qi Pan,<sup>ab</sup> Benhe Zhong,<sup>a</sup> Yonglan Luo,<sup>b</sup> Guanwei Cui,<sup>c</sup>  
Xiaodong Guo<sup>\*a</sup> and Xuping Sun<sup>†b</sup>

The conventional Haber–Bosch process for industrial NH<sub>3</sub> production from N<sub>2</sub> and H<sub>2</sub> is highly energy-intensive with a large amount of CO<sub>2</sub> emissions and finding a more suitable method for NH<sub>3</sub> synthesis under mild conditions is a very attractive topic. The electrocatalytic N<sub>2</sub> reduction reaction (NRR) offers us an environmentally benign and sustainable route. In this communication, we report that C-doped TiO<sub>2</sub> nanoparticles act as an efficient electrocatalyst for the NRR with excellent selectivity. In 0.1 M Na<sub>2</sub>SO<sub>4</sub>, it achieves an NH<sub>3</sub> yield of 16.22 μg h<sup>−1</sup> mg<sub>cat.</sub><sup>−1</sup> and a faradaic efficiency of 1.84% at −0.7 V vs. the reversible hydrogen electrode. Furthermore, this catalyst also shows good stability during electrolysis and recycling tests.

NH<sub>3</sub> is an essential ingredient in the manufacture of fertilizers, medicaments, resins, dyes, explosives, *etc.*<sup>1–4</sup> In 2017, total worldwide NH<sub>3</sub> production exceeded 150 million tons, and the demand for NH<sub>3</sub> continues to grow.<sup>5</sup> Industrially, NH<sub>3</sub> is produced almost *via* the Haber–Bosch process.<sup>6</sup> In order to overcome the kinetic limitations of strong N≡N triple bonds, elevated temperature (350–550 °C) and high pressure (150–350 atm) are necessary throughout the whole process.<sup>7–9</sup> Moreover, it not only consumes a large amount of energy, but inevitably leads to significant CO<sub>2</sub> emission. So, it is imperative to develop an environmentally friendly process for the sustainable conversion of N<sub>2</sub> to NH<sub>3</sub>.

Electrochemical NH<sub>3</sub> synthesis from N<sub>2</sub> and H<sub>2</sub>O is a promising candidate for artificial N<sub>2</sub> fixation under ambient conditions due to its environment-friendly, convenient and low-cost characteristics.<sup>10–15</sup> Although electrochemical reduction is feasible for achieving the conversion of N<sub>2</sub> to NH<sub>3</sub>, it requires

electrocatalysts for the N<sub>2</sub> reduction reaction (NRR) to meet the challenge associated with N<sub>2</sub> activation. Noble-metal catalysts such as Ru,<sup>16</sup> Au,<sup>17,18</sup> Ag,<sup>19</sup> and Rh<sup>20</sup> were reported as NRR catalysts with attractive catalytic performances, but the scarcity of these catalysts limits their wide application. Recently, transition metal oxides (TMOs)<sup>21–26</sup> have attracted much attention as NRR electrocatalysts, as they are inexpensive and can be easily prepared on a large scale. Therefore, it is still highly desirable to develop TMOs for the NRR. TiO<sub>2</sub> is nontoxic with a high thermal stability,<sup>27</sup> but its low electronic conductivity hinders its electrocatalytic application.<sup>28</sup> It has been reported that carbon doping can enhance the electronic conductivity of TiO<sub>2</sub> and facilitate charge transfer from the bulk to the surface region,<sup>29</sup> offering us a possible catalyst for the NRR, which, however, has not been explored before.

Herein, we report that C-doped TiO<sub>2</sub> nanoparticles (C-TiO<sub>2</sub>) are effective for electrochemical N<sub>2</sub> conversion to NH<sub>3</sub> with excellent selectivity under ambient conditions. In 0.1 M Na<sub>2</sub>SO<sub>4</sub>, the catalyst achieves an NH<sub>3</sub> yield of 16.22 μg h<sup>−1</sup> mg<sub>cat.</sub><sup>−1</sup> and a faradaic efficiency (FE) of 1.84% at −0.7 V vs. the reversible hydrogen electrode (RHE). Remarkably, it also demonstrates a high electrochemical stability. Compared with pristine TiO<sub>2</sub> (NH<sub>3</sub> yield: 8.49 μg h<sup>−1</sup> mg<sub>cat.</sub><sup>−1</sup>; FE: 1.28%), C-TiO<sub>2</sub> has a superior NRR performance. This result suggests that the introduction of carbon can enhance the electrocatalytic activity of TiO<sub>2</sub>.

C-TiO<sub>2</sub> nanoparticles were prepared by a facile calcination assisted solvothermal method (see the ESI† for preparation details). Fig. 1a presents the X-ray diffraction (XRD) patterns of C-TiO<sub>2</sub> and TiO<sub>2</sub>. The diffraction peaks at 25.3°, 37.8°, 48.0°, 53.9°, 55.1°, and 62.7° can be indexed to the (101), (004), (200), (105), (211), and (204) planes of anatase TiO<sub>2</sub> (JCPDS no. 21-1272), respectively, which is similar to the pattern of C-TiO<sub>2</sub>. Thermal gravimetric analysis (Fig. S1†) demonstrated that the content of C was 2.97 wt%. Scanning electron microscopy (SEM) images (Fig. S2†) indicate that the crystallite size of C-TiO<sub>2</sub> is smaller than that of TiO<sub>2</sub>. Fig. 1b shows a transmission electron microscopy (TEM) image which evidences the nanoparticle

<sup>a</sup>School of Chemical Engineering, Sichuan University, Chengdu 610065, China. E-mail: xiaodong2009@scu.edu.cn

<sup>b</sup>Institute of Fundamental and Frontier Sciences, University of Electronic Science and Technology of China, Chengdu 610054, China. E-mail: xpsun@uestc.edu.cn

<sup>c</sup>College of Chemistry, Chemical Engineering and Materials Science, Shandong Normal University, Jinan 250014, Shandong, China

† Electronic supplementary information (ESI) available: Experimental section and supplementary figures. See DOI: 10.1039/c8na00300a

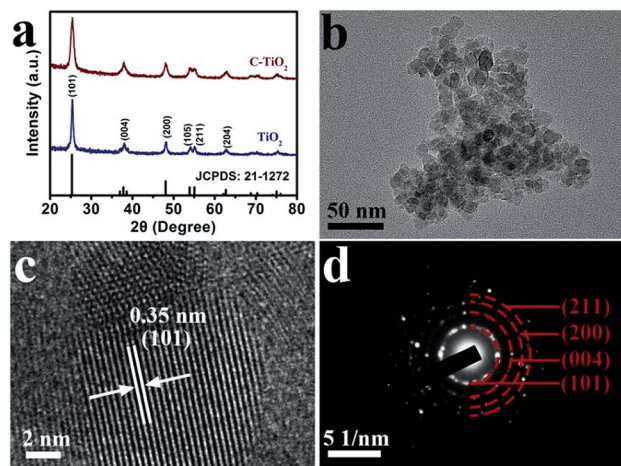


Fig. 1 (a) XRD patterns for C-TiO<sub>2</sub> and TiO<sub>2</sub>. (b) TEM and (c) HRTEM images for the C-TiO<sub>2</sub> nanoparticles. (d) SAED pattern for C-TiO<sub>2</sub>.

nature of C-TiO<sub>2</sub>. A high-resolution TEM (HRTEM) image (Fig. 1c) reveals a well-resolved lattice fringe with an interplanar distance of 0.35 nm, indexed to the (101) plane of C-TiO<sub>2</sub>. The selected area electron diffraction (SAED) pattern of C-TiO<sub>2</sub> (Fig. 1d) exhibited four diffraction rings indexed to the (101), (004), (200) and (211) planes of the TiO<sub>2</sub> phase.

Fig. 2a shows the X-ray photoelectron spectroscopy (XPS) survey spectrum of C-TiO<sub>2</sub>, which confirms the presence of Ti, C, and O elements. Fig. 2b presents the Ti 2p spectra for the C-TiO<sub>2</sub> and TiO<sub>2</sub> samples. The binding energies (BEs) of Ti 2p<sub>3/2</sub> and Ti 2p<sub>1/2</sub> for TiO<sub>2</sub> are 458.38 and 464.07 eV, respectively.<sup>30</sup> Compared to the TiO<sub>2</sub> sample, the Ti 2p peaks of C-TiO<sub>2</sub> show a positive shift of 0.3 eV, which could be attributed to lattice distortions.<sup>31</sup> Fig. 2c reveals the O 1s spectra for C-TiO<sub>2</sub> which are in good agreement with those of pure TiO<sub>2</sub>. The BEs at 529.92 and 531.33 eV in the O 1s region are ascribed to the Ti–O–Ti (lattice oxygen) and O–H bonds in C-TiO<sub>2</sub>.<sup>32,33</sup> For the C 1s

XPS spectra (Fig. 2d), three peaks can be deconvoluted at around 284.76, 286.15, and 289.12 eV for C-TiO<sub>2</sub>. The peak at 284.76 eV could be attributed to the surface adventitious carbon.<sup>30</sup> The two peaks at 286.15 and 289.12 eV are characteristic of the oxygen bound species C–O and Ti–O–C, respectively.<sup>34</sup> This result indicates that carbon atoms substitute for some of the lattice titanium atoms and form a Ti–O–C structure.<sup>30</sup> Compared with C-TiO<sub>2</sub>, only one C 1s XPS spectrum corresponding to C–C is observed for the TiO<sub>2</sub> sample, further confirming the existence of C in C-TiO<sub>2</sub>. In addition, the ultraviolet-visible (UV-vis) absorption spectra and the corresponding Kubelka–Munk plots of C-TiO<sub>2</sub> and TiO<sub>2</sub> are displayed in Fig. S3.† The band gap energies of C-TiO<sub>2</sub> (2.79 eV) and TiO<sub>2</sub> (2.96 eV) were determined by the intercept of the plots of  $(\alpha h\nu)^{1/2}$  versus photon energy ( $h\nu$ ),<sup>35</sup> indicating a narrower band gap after C doping. The enhancement of visible light absorption for C-TiO<sub>2</sub> and TiO<sub>2</sub> should be attributed to the carbon doping in the TiO<sub>2</sub> lattice, which would introduce a series of localized occupied states into the band gap of the TiO<sub>2</sub> lattice, leading to a strong visible light absorption.<sup>36</sup> All of the above results strongly support the successful preparation of C-TiO<sub>2</sub> nanoparticles.

The electrocatalytic NRR performance of C-TiO<sub>2</sub> was tested using a typical two-compartment and three-electrode device as the reaction vessel. C-TiO<sub>2</sub> was deposited on carbon paper (C-TiO<sub>2</sub>/CP with a C-TiO<sub>2</sub> loading of 0.10 mg) for the test. All of the potentials for the NRR were reported on the RHE scale. The produced NH<sub>3</sub> was detected by spectrophotometry with salicylic acid.<sup>37</sup> The relevant calibration curves are shown in Fig. S4.† The chronoamperometry curves at the corresponding potentials in N<sub>2</sub>-saturated 0.1 M Na<sub>2</sub>SO<sub>4</sub> are displayed in Fig. 3a, which can directly express the relationship between current density and time during the whole test process. Fig. 3b presents the UV-vis absorption spectra of the electrolyte stained with indophenol indicator after 2 h electrolysis at a series of potentials, and the

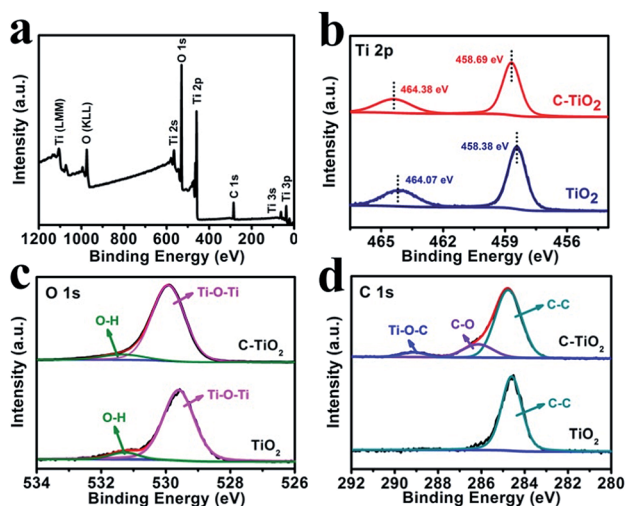


Fig. 2 (a) XPS survey spectrum for C-TiO<sub>2</sub>. XPS spectra of C-TiO<sub>2</sub> and TiO<sub>2</sub> in the (b) Ti 2p, (c) O 1s and (d) C 1s regions.

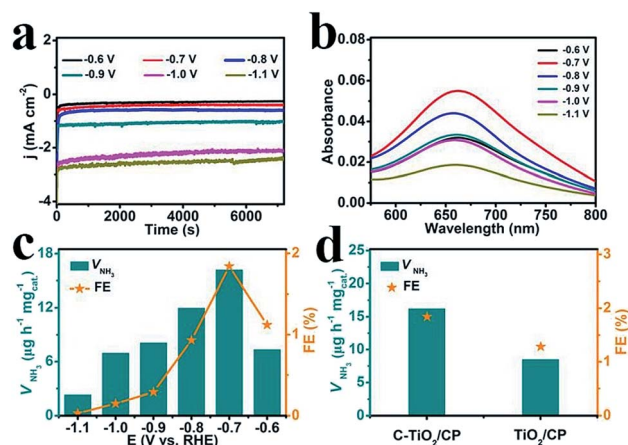


Fig. 3 (a) Chronoamperometry curves at the corresponding potentials in N<sub>2</sub>-saturated 0.1 M Na<sub>2</sub>SO<sub>4</sub>. (b) UV-vis absorption spectra of the electrolyte stained with indophenol indicator after 2 h electrolysis at a series of potentials. (c) The NH<sub>3</sub> yields and FEs of C-TiO<sub>2</sub> for the NRR at a series of potentials. (d) The amount of NH<sub>3</sub> with different electrodes at -0.7 V after 2 h electrolysis under ambient conditions.



values of absorbance at 660 nm were used to calculate the concentrations of the generated  $\text{NH}_3$  at different applied potentials according to the calibration curve of  $\text{NH}_3$ . Combined with the collected data, the final results including the  $\text{NH}_3$  yields and FEs under various potentials were calculated and are plotted in Fig. 3c. Both the  $\text{NH}_3$  yields and FEs increase as the negative potential rises to  $-0.7$  V, which is the optimum potential point when the  $\text{NH}_3$  yield and FE are  $16.22 \mu\text{g h}^{-1} \text{mg}_{\text{cat}}^{-1}$  and 1.84%, respectively. After that, as the potential continually increases, both the  $\text{NH}_3$  yields and FEs decrease significantly which is mainly caused by the competitive hydrogen evolution reaction. For comparison, the pure  $\text{TiO}_2$  sample was tested under the same conditions and the corresponding results are presented in Fig. 3d. It is worth noting that the performance of C-TiO<sub>2</sub> is evidently better than that of pure  $\text{TiO}_2$ . The superior NRR performance of C-TiO<sub>2</sub> can be rationally attributed to the C-TiO<sub>2</sub> nanoparticles having more exposed active sites (Fig. S5†), enabling more effective utilization of them as electrocatalysts. The enhanced conductivity of C-TiO<sub>2</sub> also contributes to its higher catalytic activity. The charge transfer resistance related to the electrocatalytic kinetics can be determined from the diameter of the semicircles in the low frequency zone.<sup>38</sup> Electrochemical impedance spectroscopy data (Fig. S6†) show that C-TiO<sub>2</sub>/CP possesses a smaller radius of the semicircle compared to  $\text{TiO}_2$ /CP, suggesting that the C-TiO<sub>2</sub> sample has a lower charge transfer resistance<sup>39</sup> and thus faster NRR kinetics. Meanwhile, C-TiO<sub>2</sub> shows a higher performance than some of the previously reported NRR electrocatalysts.<sup>40–44</sup> More detailed comparisons are listed in Table S1.†

To prove that  $\text{NH}_3$  was generated *via* the  $\text{N}_2$  reduction process of C-TiO<sub>2</sub>, three sets of control experiments were carried out: (1) immersing the samples in Ar-saturated solution at  $-0.7$  V for 2 h; (2) immersing the samples in  $\text{N}_2$ -saturated solution at an open circuit potential for 2 h; and (3) immersing the samples at  $-0.7$  V with alternating 2 h cycles between  $\text{N}_2$ -

saturated and Ar-saturated solutions, for a total of 12 h. As shown in Fig. 4a and Fig. S7,† a trace amount of  $\text{NH}_3$  production was detected under Ar-saturated solution and an open circuit potential. Combined with Fig. S8,† this result indicates that only  $\text{N}_2$  provides the nitrogen source to  $\text{NH}_3$ . Moreover, controlled trials were carried out to investigate the performance of bare CP. The relevant UV-vis absorption spectra are displayed in Fig. S9.† The results show the poor electrocatalytic activity of bare CP, indicating that C-TiO<sub>2</sub> is an active material for the NRR (Fig. 4b). In addition, stable performance is another important indicator for evaluating catalysts. Recycling tests were performed in  $\text{N}_2$ -saturated 0.1 M  $\text{Na}_2\text{SO}_4$  6 times and the results are shown in Fig. 4c. The  $\text{NH}_3$  yield and FE results show no obvious fluctuation over the whole process, suggesting that C-TiO<sub>2</sub> possesses a stable NRR performance. Moreover, only a slight fluctuation of current density is observed at  $-0.7$  V after 24 h electrolysis, further suggesting an excellent electrochemical stability.

Hydrazine ( $\text{N}_2\text{H}_4$ ), as a possible by-product in the NRR test, was detected by the method of Watt and Chrisp.<sup>45</sup> The relevant calibration curves are displayed in Fig. S10.† The UV-vis absorption spectra of  $\text{N}_2\text{H}_4$  after 2 h electrolysis in a  $\text{N}_2$  atmosphere at a series of potentials are shown in Fig. S11.† The concentrations of the possible by-product  $\text{N}_2\text{H}_4$  are determined according to the values of absorbance at 455 nm. The results demonstrated that no  $\text{N}_2\text{H}_4$  was detected at all potentials, implying the excellent selectivity of C-TiO<sub>2</sub> as an NRR electrocatalyst.

In summary, C-TiO<sub>2</sub> nanoparticles have been proven as an effective non-noble-metal electrocatalyst for the NRR at moderate temperatures and atmospheric pressure. This electrocatalyst achieves an  $\text{NH}_3$  yield of  $16.22 \mu\text{g h}^{-1} \text{mg}_{\text{cat}}^{-1}$  and a FE of 1.84% at  $-0.7$  V vs. RHE in 0.1 M  $\text{Na}_2\text{SO}_4$ . It also exhibits excellent selectivity and satisfactory electrochemical stability during the process of electrochemical  $\text{NH}_3$  synthesis under ambient conditions. This work not only offers us an attractive earth-abundant electrocatalyst for the NRR, but also opens up an exciting new avenue for the design and development of doped Ti-based catalysts<sup>46,47</sup> with enhanced performances toward electrocatalytic  $\text{N}_2$  and nitrite<sup>48</sup> reduction for applications.

## Conflicts of interest

There are no conflicts to declare.

## Acknowledgements

The authors would like to thank the National Natural Science Foundation of China (No. 21506133) and the Youth Foundation of Sichuan University (No. 2017SCU04a08) for their support in this research.

## References

- 1 R. Schlögl, *Angew. Chem., Int. Ed.*, 2003, **42**, 2004–2008.

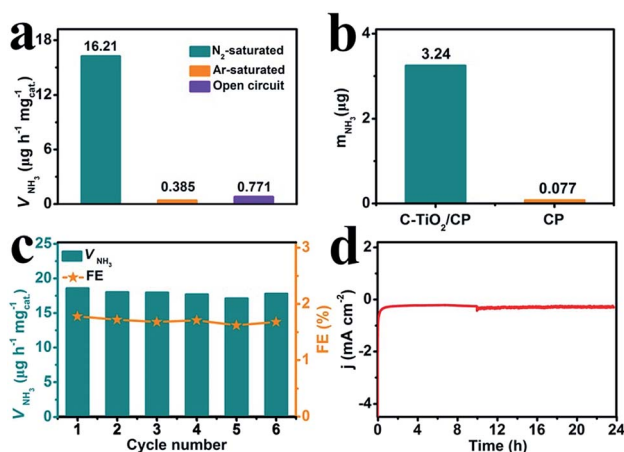


Fig. 4 (a)  $\text{NH}_3$  yields for C-TiO<sub>2</sub> under different conditions. (b) The amount of  $\text{NH}_3$  with different electrodes at  $-0.7$  V after 2 h electrolysis under ambient conditions. (c)  $\text{NH}_3$  yields and FEs at a potential of  $-0.7$  V during 6 recycling tests. (d) Chronoamperometry curve at a potential of  $-0.7$  V using a C-TiO<sub>2</sub>/CP catalyst for 24 h.





- 2 T. Murakami, T. Nishikiori, T. Nohira and Y. Ito, *J. Am. Chem. Soc.*, 2003, **125**, 334–335.
- 3 V. Rosca, M. Duca, M. T. de Groot and M. T. Koper, *Chem. Rev.*, 2009, **109**, 2209–2244.
- 4 C. Guo, J. Ran, A. Vasileff and S. Qiao, *Energy Environ. Sci.*, 2018, **11**, 45–56.
- 5 J. A. Ober, *Mineral Commodity Summaries 2018*, ed. S. M. Kimball, U.S. Geological Survey, U.S. Government Printing Office, Washington, DC, 2018, DOI: 10.3133/70194932.
- 6 V. Smil, *Nature*, 1999, **400**, 415.
- 7 G. Ertl, *Catalytic ammonia synthesis*, ed. J. R. Jennings, Plenum, New York, 1991.
- 8 C. J. M. van der Ham, M. T. M. Koper and D. G. H. Hetterscheid, *Chem. Soc. Rev.*, 2014, **43**, 5183–5191.
- 9 G. Chen, X. Cao, S. Wu, X. Zeng, L. Ding, M. Zhu and H. Wang, *J. Am. Chem. Soc.*, 2017, **139**, 9771–9774.
- 10 L. Zhang, X. Ji, X. Ren, Y. Ma, X. Shi, Z. Tian, A. M. Asiri, L. Chen, B. Tang and X. Sun, *Adv. Mater.*, 2018, **30**, 1800191.
- 11 X. Ren, G. Cui, L. Chen, F. Xie, Q. Wei, Z. Tian and X. Sun, *Chem. Commun.*, 2018, **54**, 8474–8477.
- 12 L. Zhang, X. Ji, X. Ren, Y. Luo, X. Shi, A. M. Asiri, B. Zheng and X. Sun, *ACS Sustainable Chem. Eng.*, 2018, **6**, 9550–9554.
- 13 X. Li, T. Li, Y. Ma, Q. Wei, W. Qiu, H. Guo, X. Shi, P. Zhang, A. M. Asiri, L. Chen, B. Tang and X. Sun, *Adv. Energy Mater.*, 2018, **8**, 1801357.
- 14 W. Qiu, X. Xie, J. Qiu, W. Fang, R. Liang, X. Ren, X. Ji, G. Cui, A. M. Asiri, G. Cui, B. Tang and X. Sun, *Nat. Commun.*, 2018, **9**, 3485.
- 15 R. Zhang, Y. Zhang, X. Ren, G. Cui, A. M. Asiri, B. Zheng and X. Sun, *ACS Sustainable Chem. Eng.*, 2018, **6**, 9545–9549.
- 16 V. Kordali, G. Kyriacou and C. Lambrou, *Chem. Commun.*, 2000, **17**, 1673–1674.
- 17 M. Shi, D. Bao, B. Wulan, Y. Li, Y. Zhang, J. Yan and Q. Jiang, *Adv. Mater.*, 2017, **29**, 1606550.
- 18 D. Bao, Q. Zhang, F. Meng, H. Zhong, M. Shi, Y. Zhang, J. Yan, Q. Jiang and X. Zhang, *Adv. Mater.*, 2017, **29**, 1604799.
- 19 H. Huang, L. Xia, X. Shi, A. M. Asiri and X. Sun, *Chem. Commun.*, 2018, **54**, 11427–11430.
- 20 H. Liu, S. Han, Y. Zhao, Y. Zhu, X. Tian, J. Zeng, J. Jiang, B. Xia and Y. Chen, *J. Mater. Chem. A*, 2018, **6**, 3211–3217.
- 21 C. Lv, C. Yan, G. Chen, Y. Ding, J. Sun, Y. Zhou and G. Yu, *Angew. Chem., Int. Ed.*, 2018, **57**, 6073–6076.
- 22 L. Zhang, X. Ren, Y. Luo, X. Shi, A. M. Asiri, T. Li and X. Sun, *Chem. Commun.*, 2018, **54**, 12966–12969.
- 23 S. Chen, S. Perathoner, C. Ampelli, C. Mebrahtu, D. Su and G. Centi, *Angew. Chem., Int. Ed.*, 2017, **56**, 2699–2703.
- 24 Q. Liu, X. Zhang, B. Zhang, Y. Luo, G. Cui, F. Xie and X. Sun, *Nanoscale*, 2018, **10**, 14386–14389.
- 25 J. Han, X. Ji, X. Ren, G. Cui, L. Li, F. Xie, H. Wang, B. Li and X. Sun, *J. Mater. Chem. A*, 2018, **6**, 12974–12977.
- 26 Z. Wang, F. Gong, L. Zhang, R. Wang, L. Ji, Q. Liu, Y. Luo, H. Guo, Y. Li, P. Gao, X. Shi, B. Li, B. Tang and X. Sun, *Adv. Sci.*, 2018, **5**, 1801182.
- 27 J. Du, X. Lai, N. Yang, J. Zhai, D. Kisailus, F. Su, D. Wang and L. Jiang, *ACS Nano*, 2011, **5**, 590–596.
- 28 W. Li, Y. Bai, F. Li, C. Liu, K. Chan, X. Feng and X. Lu, *J. Mater. Chem.*, 2012, **22**, 4025–4031.
- 29 J. Shao, W. Sheng, M. Wang, S. Li, J. Chen, Y. Zhang and S. Cao, *Appl. Catal., B*, 2017, **209**, 311–319.
- 30 W. Ren, Z. Ai, F. Jia, L. Zhang, X. Fan and Z. Zou, *Appl. Catal., B*, 2007, **69**, 138–144.
- 31 E. M. Neville, M. J. Mattle, D. Loughrey, B. Rajesh, M. Rahman, J. M. D. MacElroy, J. A. Sullivan and K. R. Thampi, *J. Phys. Chem. C*, 2012, **116**, 16511–16521.
- 32 B. Li, Z. Zhao, F. Gao, X. Wang and J. Qiu, *Appl. Catal., B*, 2014, **147**, 958–964.
- 33 C. Yang, X. Zhang, J. Qin, X. Shen, R. Yu, M. Ma and R. Liu, *J. Catal.*, 2017, **347**, 36–44.
- 34 Y. Zhang, Z. Zhao, J. Chen, L. Cheng, J. Chang, W. Sheng, C. Hu and S. Cao, *Appl. Catal., B*, 2015, **165**, 715–722.
- 35 C. Chen, M. Long, H. Zeng, W. Cai, B. Zhou, J. Zhang, Y. Wu, D. Ding and D. Wu, *J. Mol. Catal. A: Chem.*, 2009, **314**, 35–41.
- 36 C. D. Valentin, G. Pacchioni and A. Selloni, *Chem. Mater.*, 2005, **17**, 6656–6665.
- 37 D. Zhu, L. Zhang, R. E. Ruther and R. J. Hamers, *Nat. Mater.*, 2013, **12**, 836–841.
- 38 Y. Zhu, Y. Liu, T. Ren and Z. Yuan, *Adv. Funct. Mater.*, 2015, **25**, 7337–7347.
- 39 C. Guo, L. Zhang, J. Miao, J. Zhang and C. Li, *Adv. Energy Mater.*, 2013, **3**, 167–171.
- 40 Y. Liu, Y. Su, X. Quan, X. Fan, S. Chen, H. Yu, H. Zhao, Y. Zhang and J. Zhao, *ACS Catal.*, 2018, **8**, 1186–1191.
- 41 D. Yang, T. Chen and Z. Wang, *J. Mater. Chem. A*, 2017, **5**, 18967–18971.
- 42 J. Kong, A. Lim, C. Yoon, J. H. Jang, H. C. Ham, J. Han, S. Nam, D. Kim, Y. Sung, J. Choi and H. S. Park, *ACS Sustainable Chem. Eng.*, 2017, **5**, 10986–10995.
- 43 M. Shi, D. Bao, S. Li, B. Wulan, J. Yan and Q. Jiang, *Adv. Energy Mater.*, 2018, **8**, 1800124.
- 44 X. Xiang, Z. Wang, X. Shi, M. Fan and X. Sun, *ChemCatChem*, 2018, **10**, 1–7.
- 45 G. W. Watt and J. D. Chrisp, *Anal. Chem.*, 1952, **24**, 2006–2008.
- 46 R. Zhang, X. Ren, X. Shi, F. Xie, B. Zheng, X. Guo and X. Sun, *ACS Appl. Mater. Interfaces*, 2018, **10**, 28251–28255.
- 47 X. Zhang, Q. Liu, X. Shi, A. M. Asiri, Y. Luo, X. Sun and T. Li, *J. Mater. Chem. A*, 2018, **6**, 17303–17306.
- 48 R. Wang, Z. Wang, X. Xiang, R. Zhang, X. Shi and X. Sun, *Chem. Commun.*, 2018, **54**, 10340–10342.

